Supplementary Information

Controlling Metastability through Annealing of High-Entropy Nanoalloy Electrocatalysts to Boost Performance towards the Oxygen Evolution Reaction

Varatharaja Nallathambi[1,2*], Aneeta Jose Puthussery[3,4], Andrea M. Mingers[2], Robert Stuckert[1], André Olean-Oliveira[3,4], Sven Reichenberger[1], Dierk Raabe[2], Viktor Čolić[3,4], Baptiste Gault[2,5*], Stephan Barcikowski[1]

[1] Technical Chemistry I and Center for Nanointegration Duisburg-Essen (CENIDE), University of Duisburg-Essen, Universitaetsstr. 7, 45141 Essen, Germany

[2] Max Planck Institute for Sustainable Materials, Max-Planck-Str. 1, 40237 Düsseldorf, Germany

[3] Max Planck Institute for Chemical Energy Conversion, Stiftstr.34-36, 45470 Mülheim an der Ruhr, Germany

[4] CENIDE─Center for Nanointegration Duisburg-Essen, Carl-Benz-Str. 199, 47057 Duisburg, Germany

[5] Univ Rouen Normandie, CNRS, INSA Rouen Normandie, Groupe de Physique des Matériaux, UMR 6634, F-76000 Rouen, France

* corresponding authors: v.nallathambi@mpi-susmat.de, baptiste.gault1@univ-rouen.fr

Keywords: High-entropy alloys, compositionally complex alloys, oxygen evolution reaction, laser ablation, electrocatalysis, heterostructures, annealing, *in situ* TEM heating

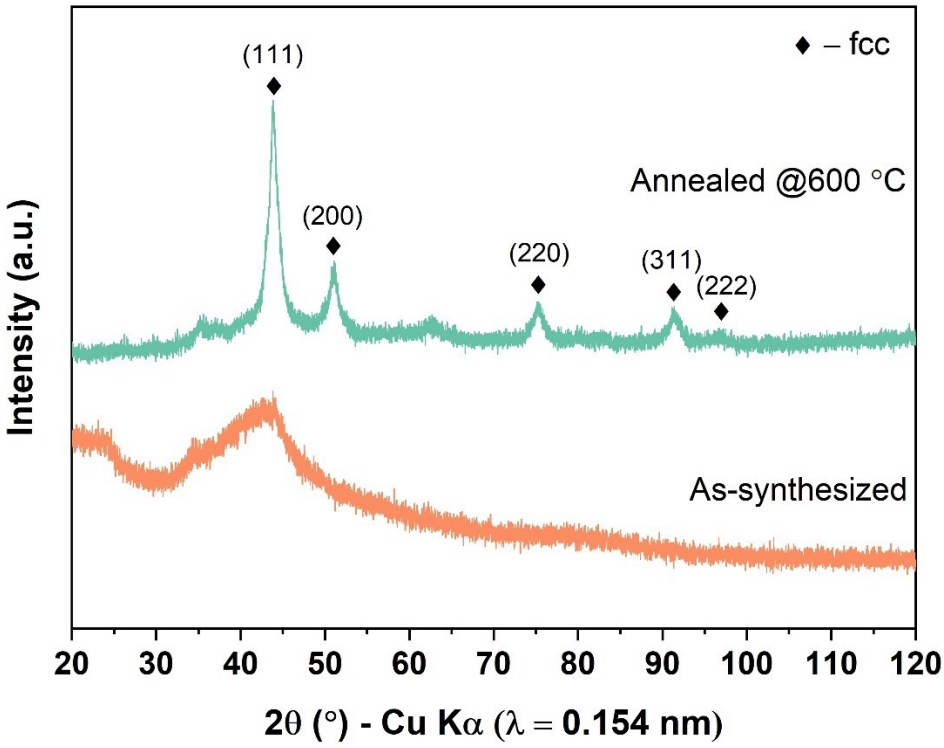

Figure S1 XRD patterns of as-synthesized amorphous and annealed crystalline HEA NPs. Strong reflections of an fcc phase can be observed for the annealed sample with minor reflections at ~35° and ~63° which could be attributed to surface oxides.

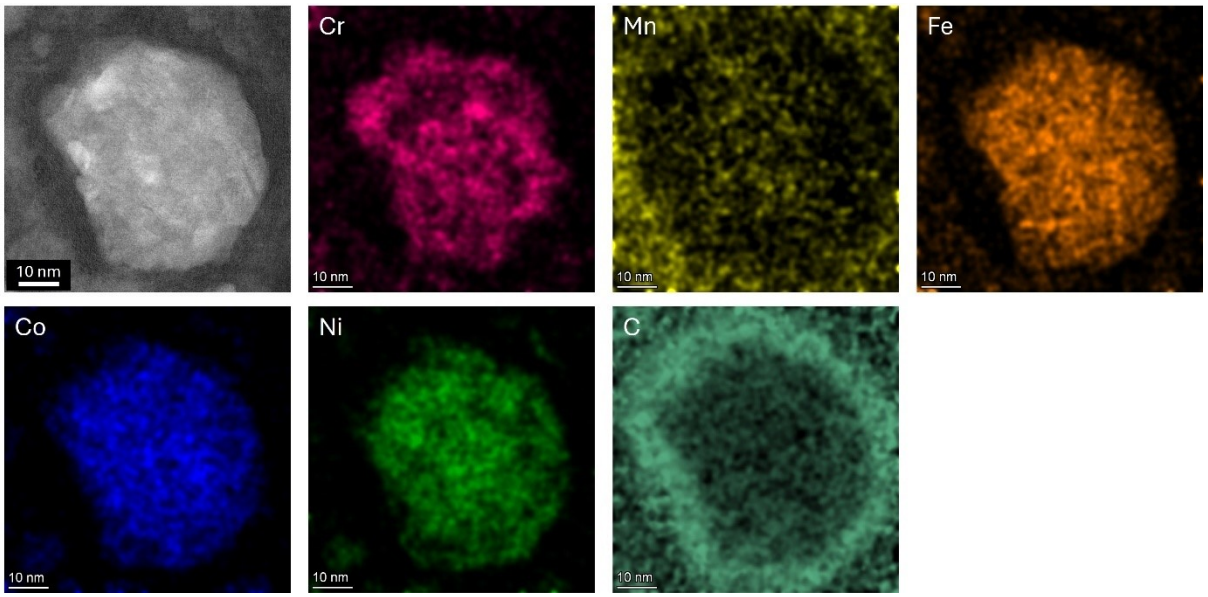

Figure S2 STEM dark field image and corresponding EDS mappings of the constituent elements of a HEA NP synthesized in acetone annealed at 600 °C.

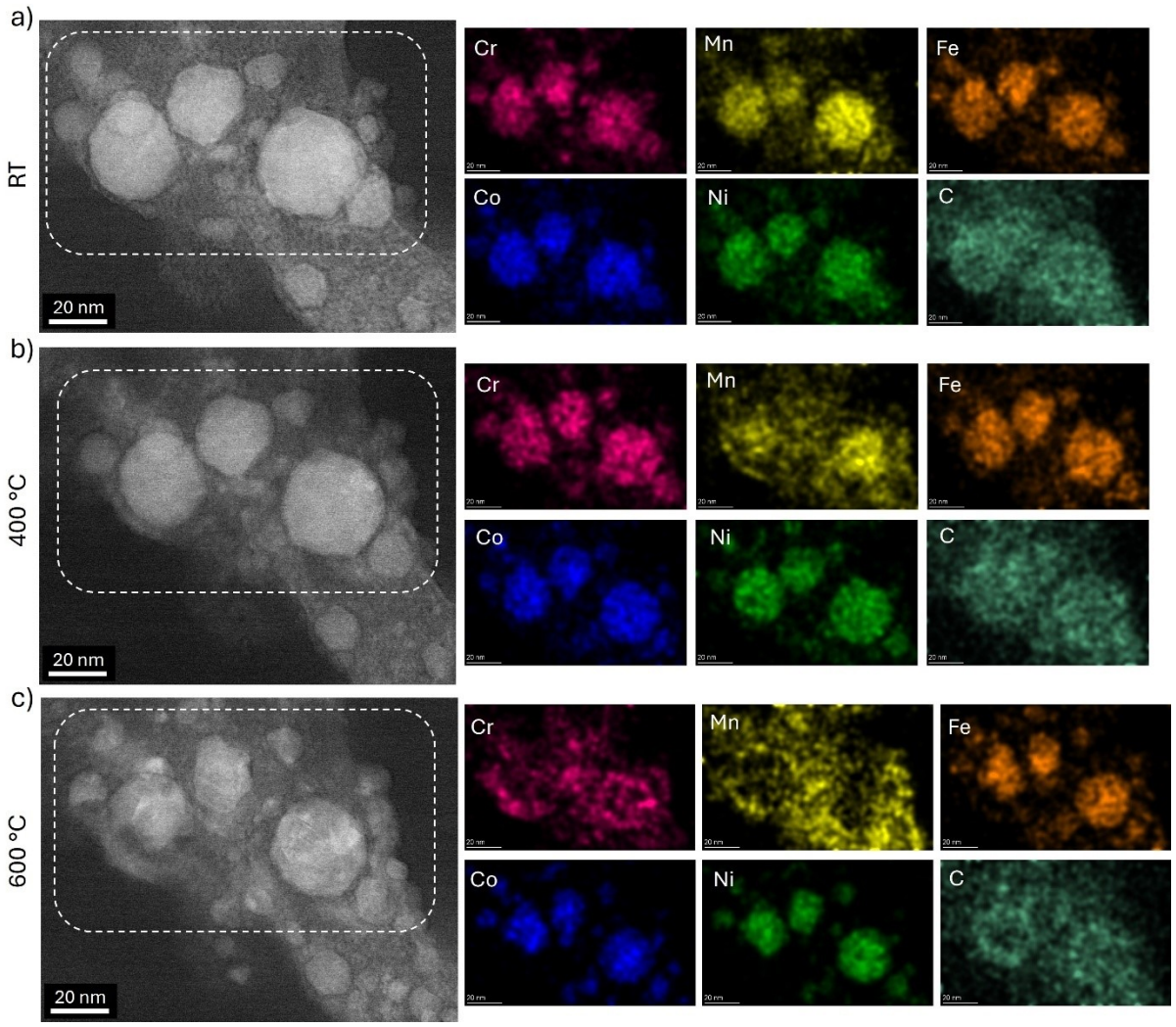

Figure S3 a), b), c) STEM dark field image and corresponding EDS mappings of the constituent elements of the HEA NPs synthesized in acetone at RT, annealed at 400 °C and 600 °C, respectively.

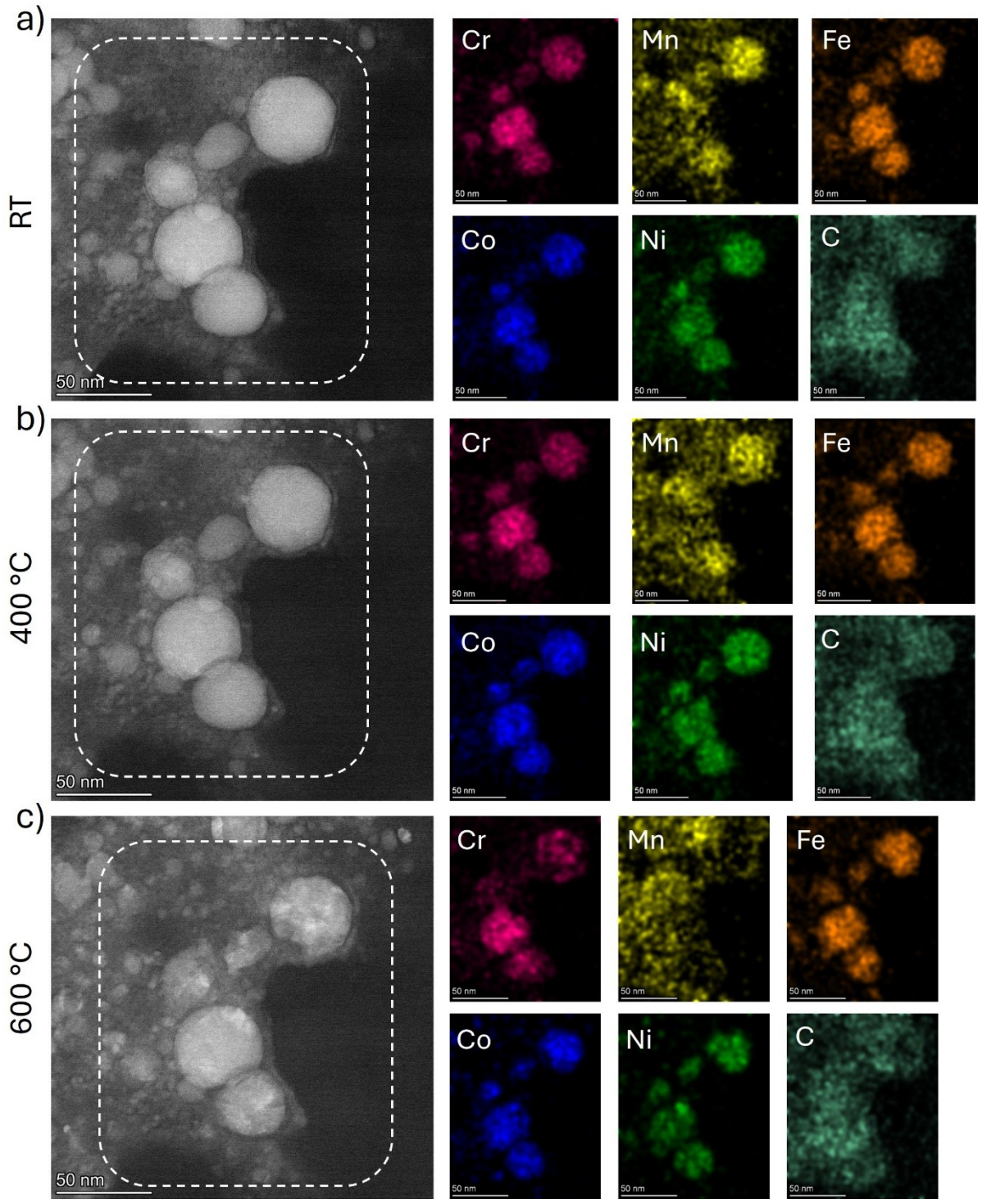

Figure S4 a), b), c) STEM dark field image and corresponding EDS mappings of the constituent elements of the HEA NPs synthesized in acetone at RT, annealed at 400 °C and 600 °C, respectively.

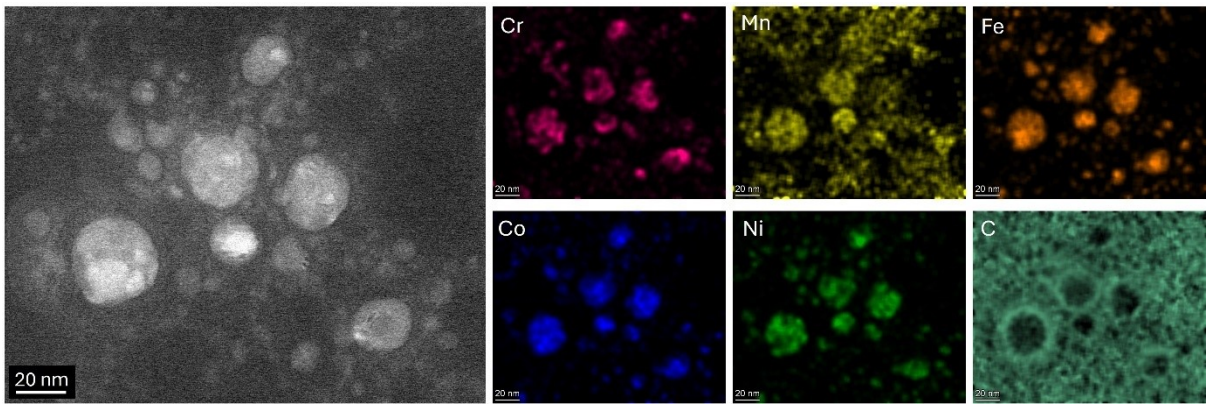

Figure S5 STEM-EDS mappings of HEA NPs synthesized in acetonitrile annealed at 600 °C.

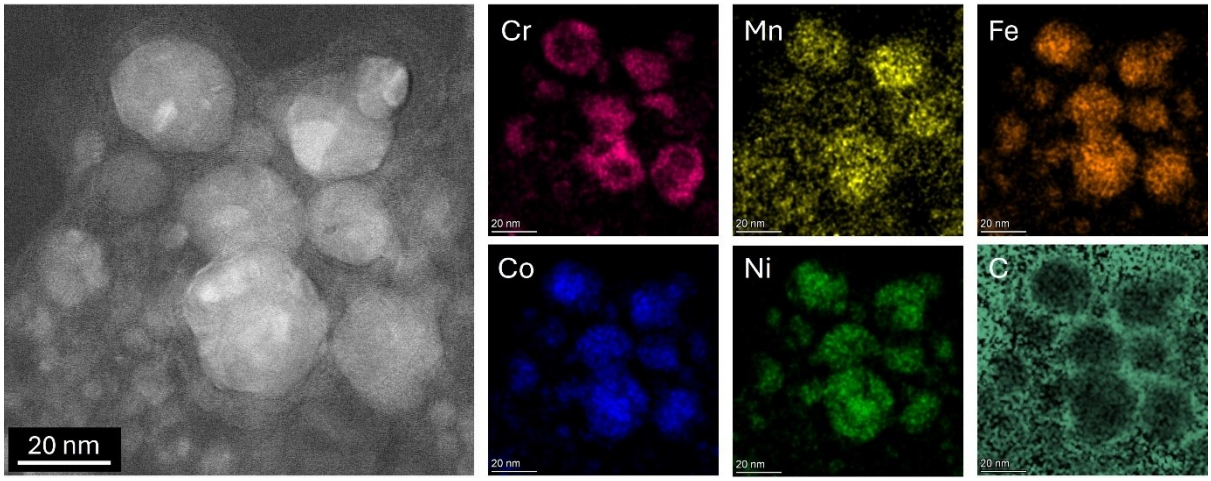

Figure S6 STEM-EDS mappings of HEA NPs synthesized in acetonitrile annealed at 600 °C.

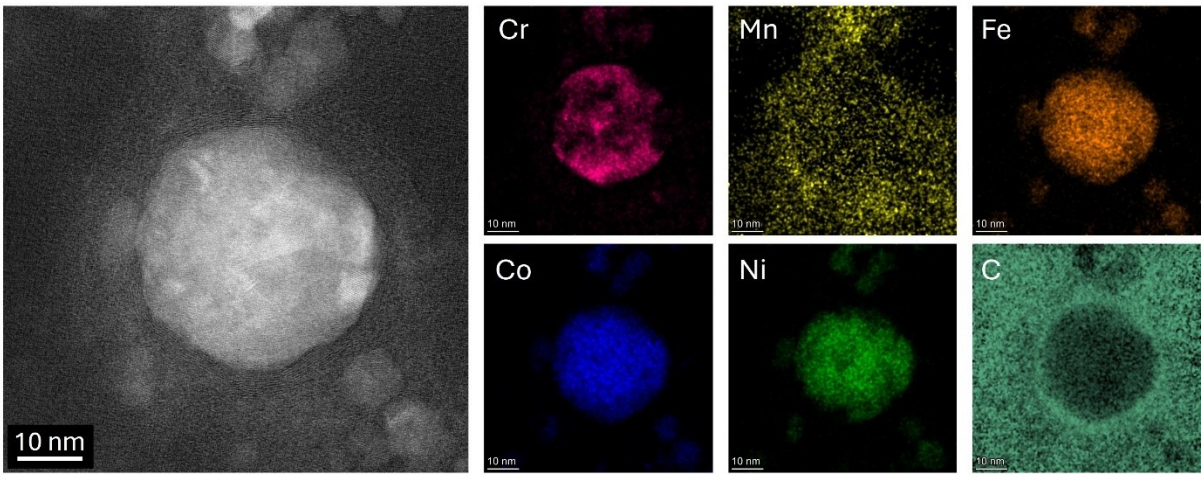

Figure S7 STEM-EDS mappings of HEA NPs synthesized in acetonitrile annealed at 600 °C.

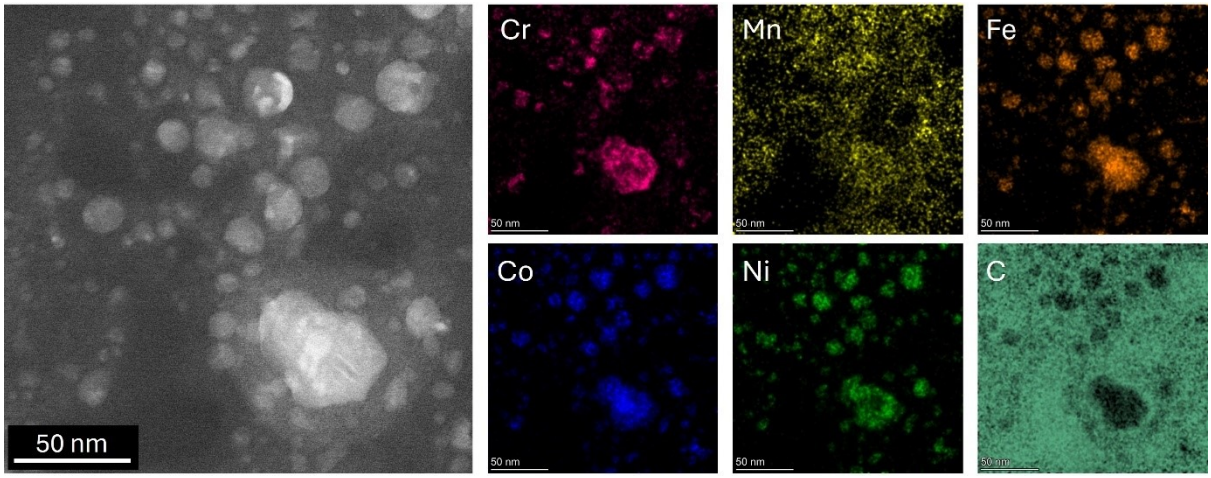

Figure S8 STEM-EDS mappings of HEA NPs synthesized in acetonitrile annealed at 600 °C.

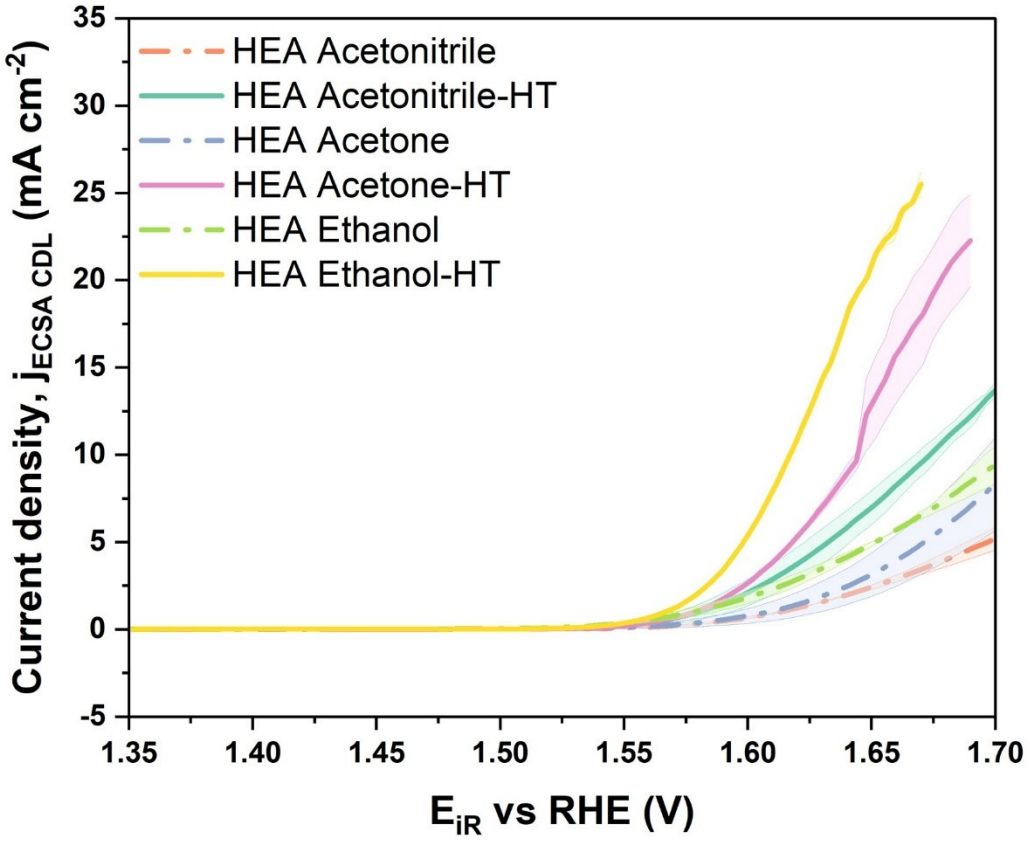

Figure S9 Linear sweep voltametry curves (current density normalized with ECSA) of the as-synthesized and annealed (denoted as HT) HEA NPs synthesized in acetonitrile, acetone and ethanol, respectively.

The EIS data were fitted using the equivalent electric circuit (EEC) shown in the inset of Figure S10. The model consists of the components arranged in $R_s + Q_{dl} / (R_{ct} + C_a + R_a)$, where R1 or R_s is the solution resistance, Q1 or Q_{dl} corresponds to the double layer capacitance. R2 or R_{ct} represents the charge transfer resistance. C1 (C_a) and R3 (Ra) represent the adsorption capacitance and adsorption resistance. In this model constant phase element (Q) is used instead of capacitance in order to count for the non-ideal behavior. The coefficient *a* reflects the deviation from the ideal behavior [1,2].

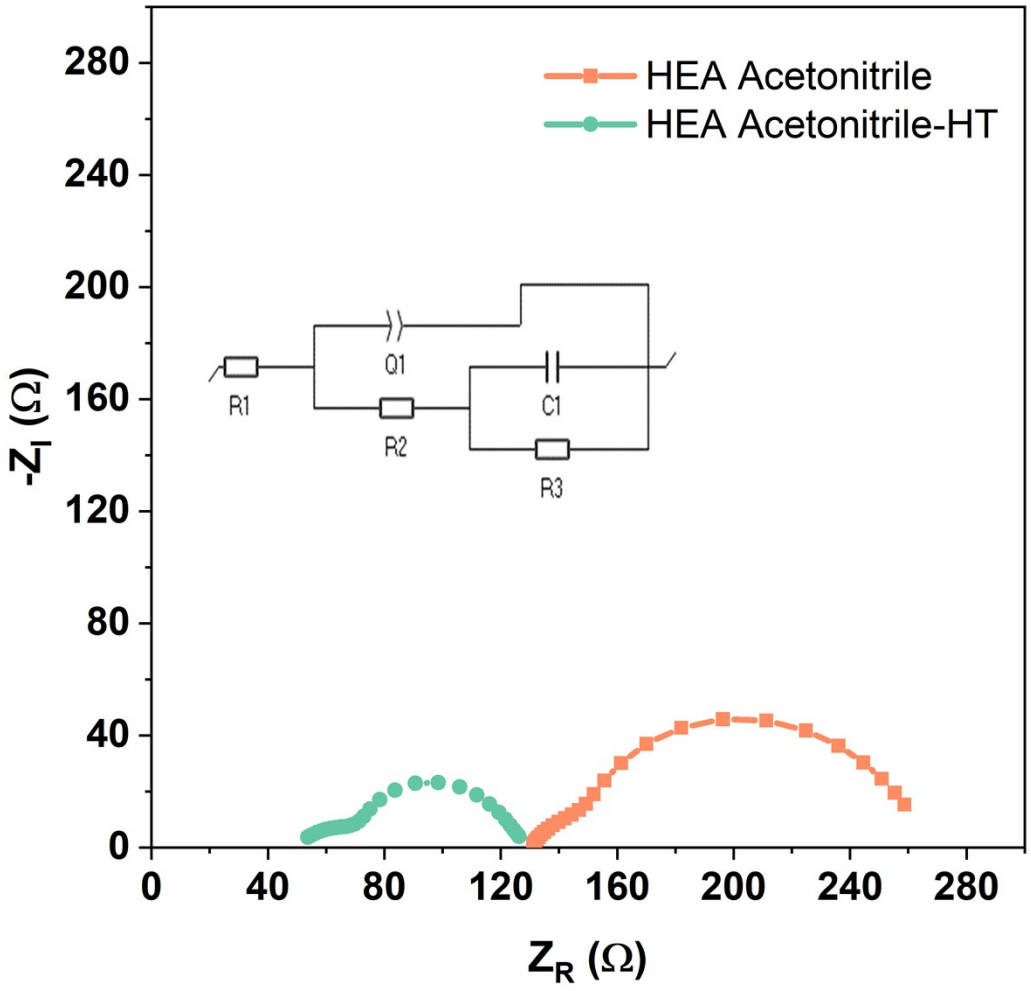

Figure S10 Nyquist plots for the as-synthesized and annealed HEA NPs synthesized in acetonitrile with the equivalent circuit for the spectrum given in the inset. The experiment was carried out at 1.6 V in 0.1 M KOH. Frequency range: 1Hz – 30kHz with 10 mV amplitude and 6 step dec^{-1}.

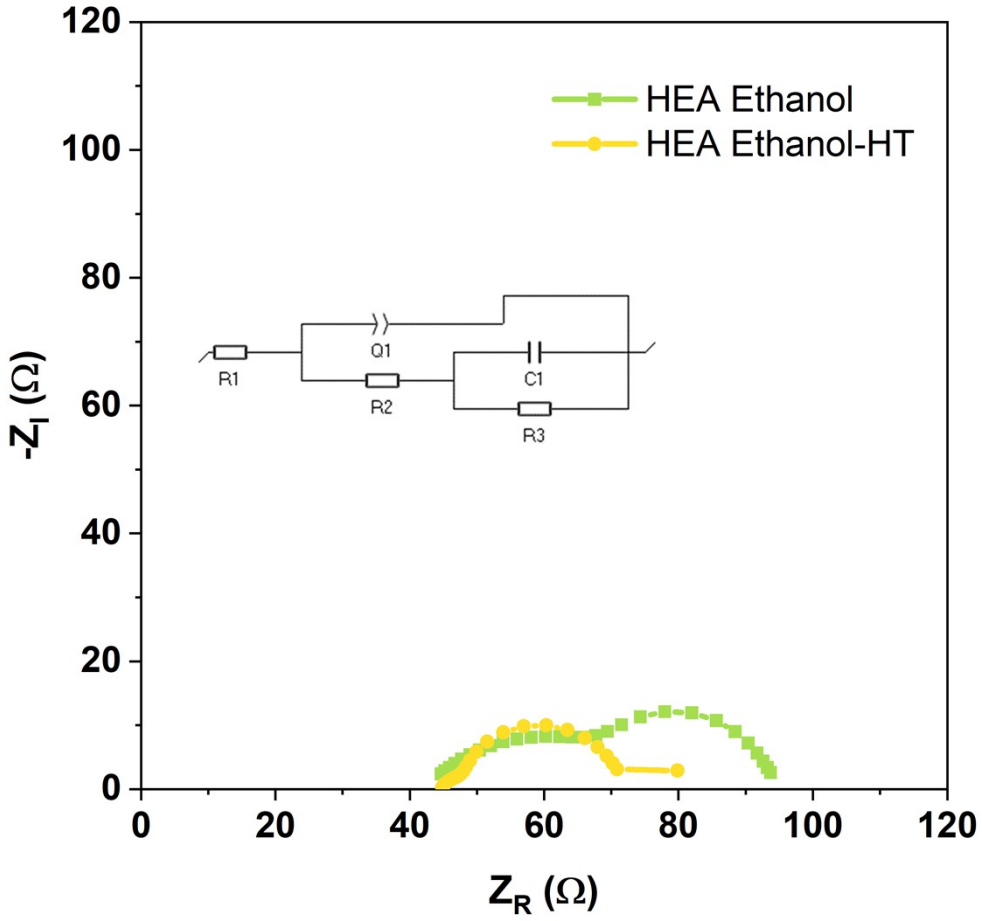

Figure S11 Nyquist plots for the as-synthesized and annealed HEA NPs synthesized in ethanol with the equivalent circuit for the spectrum given in the inset. The experiment was carried out at 1.6 V in 0.1 M KOH. Frequency range: 1Hz – 30kHz with 10 mV amplitude and 6 step dec^{-1}.

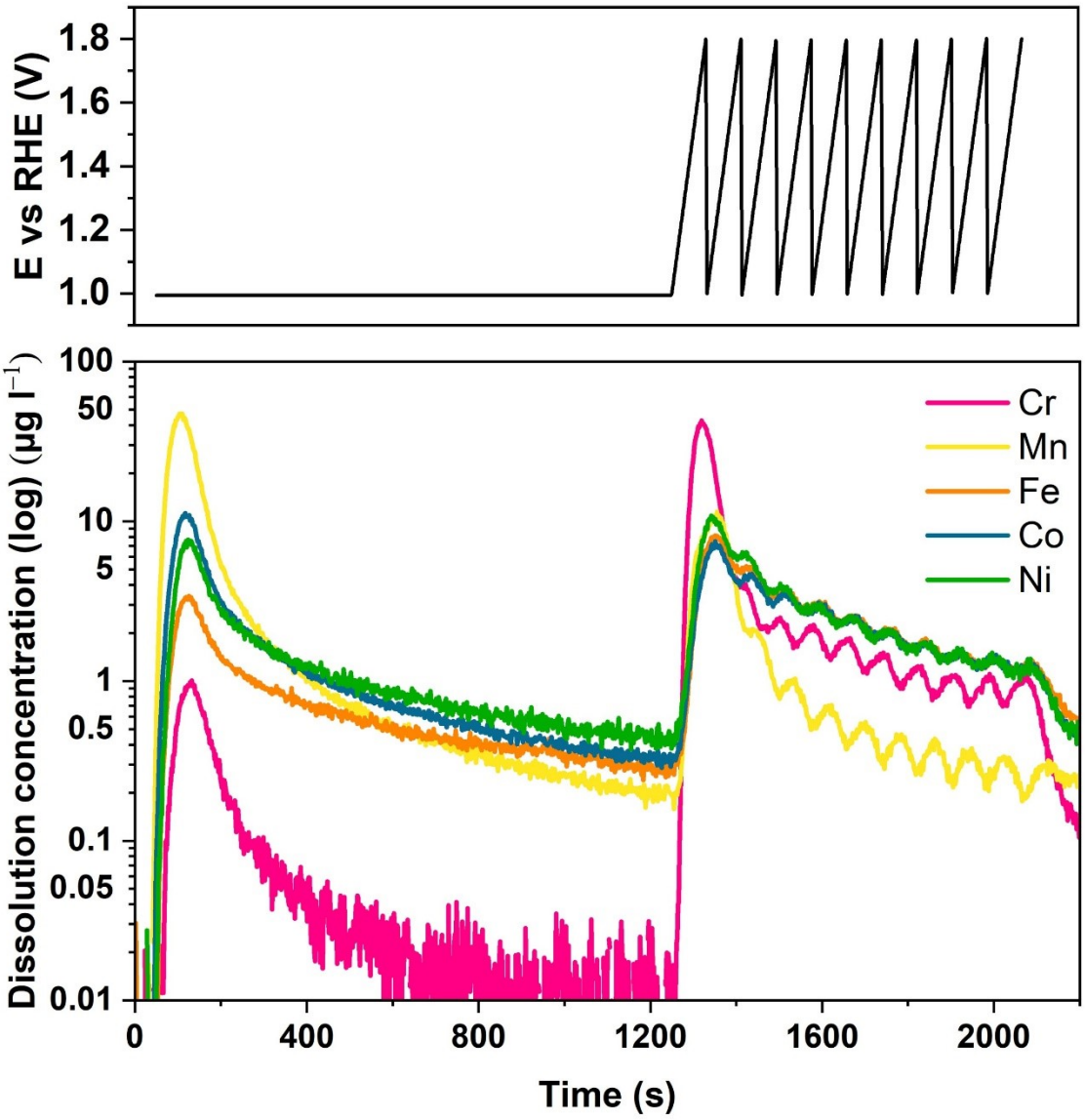

Figure S12 Applied potential and the corresponding online ICP-MS dissolution profiles of dissolved metal ions as a function of time of the annealed HEA NPs in acetonitrile.

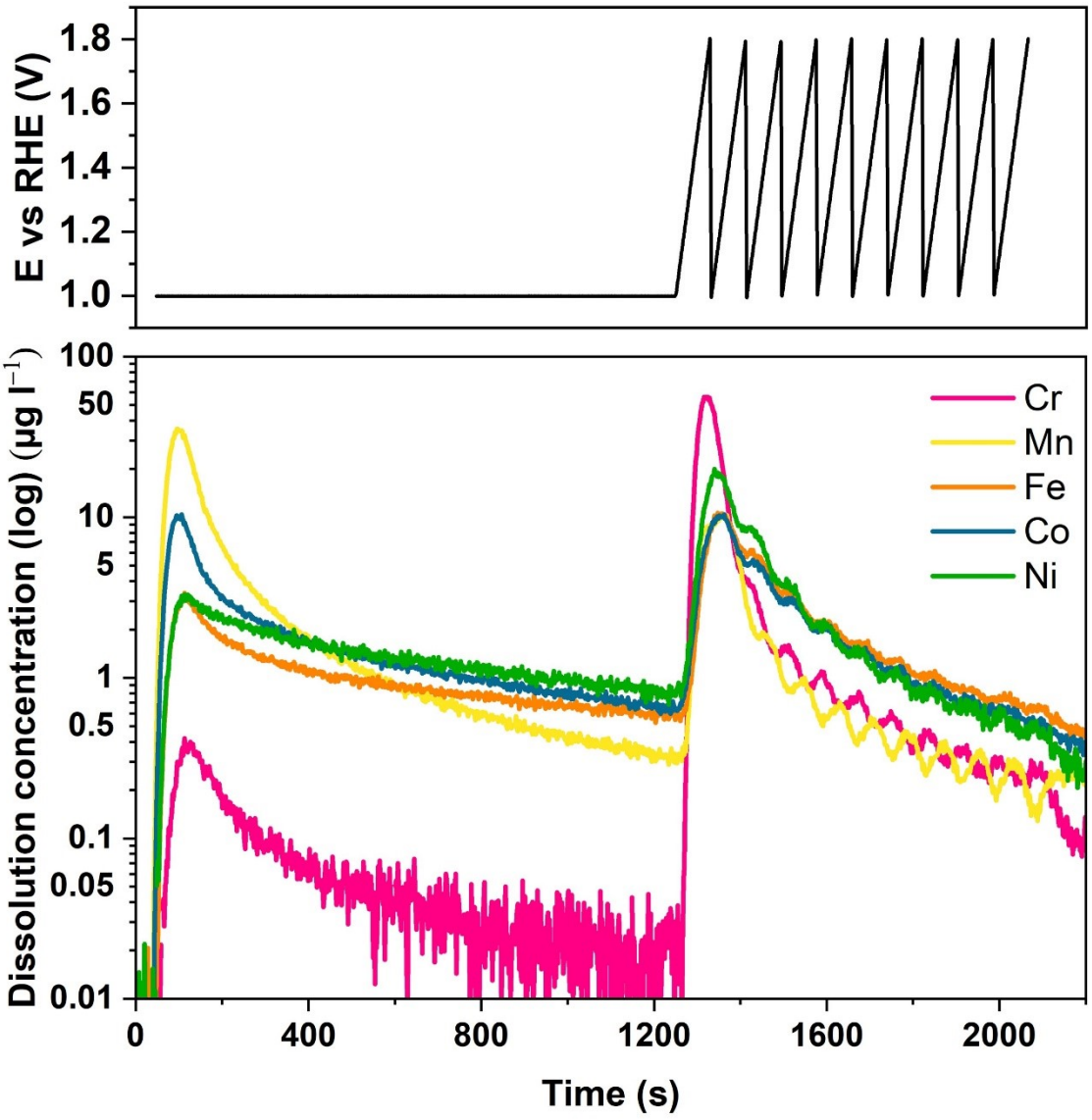

Figure S13 Applied potential and the corresponding online ICP-MS dissolution profiles of dissolved metal ions as a function of time of the annealed HEA NPs in ethanol.

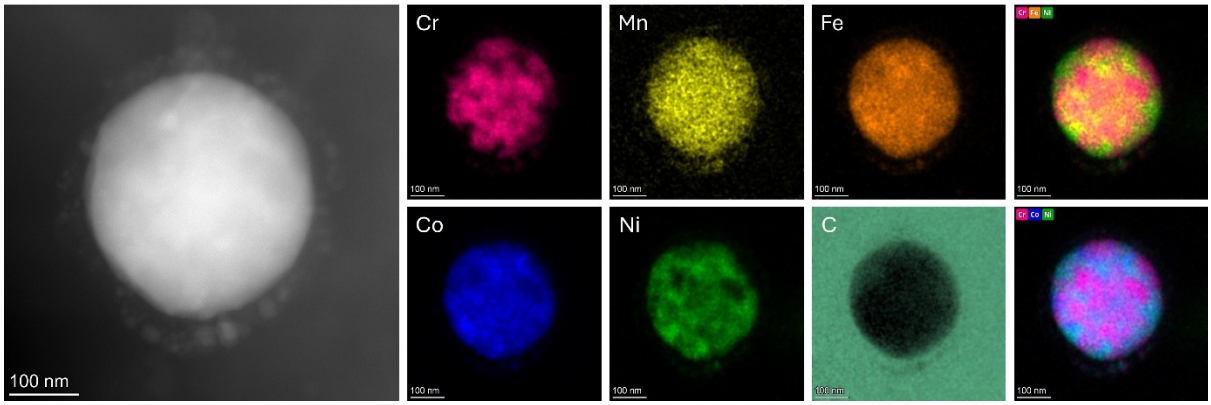

Figure S14 STEM-EDS mapping and corresponding Cr-Fe-Ni and Cr-Co-Ni elemental mapping overlays of an annealed HEA NP (~320 nm in diameter) synthesized in acetone after OER cycling, highlighting the retention of the heterostructured microstructure after electrochemical testing.

Table S1 Constraints used during the peak fitting of XPS 3p spectra listed for each element.

	Cr 3p		Mn 3p		Fe 3p		Co 3p_#1	
	min	max	min	max	min	max	min	max
Pos. Constr. / eV	46	47	47	50.4	53.7	56.7	59.9	62.5
FWHM Constr. / eV	0.6	5	0.6	5	0.6	5	0.6	5

	Co 3p_#2		Ni 3p	
	min	max	min	max
Pos. Constr. / eV	59.8	64.5	67.5	69
FWHM Constr. / eV	0.6	2	0.6	5

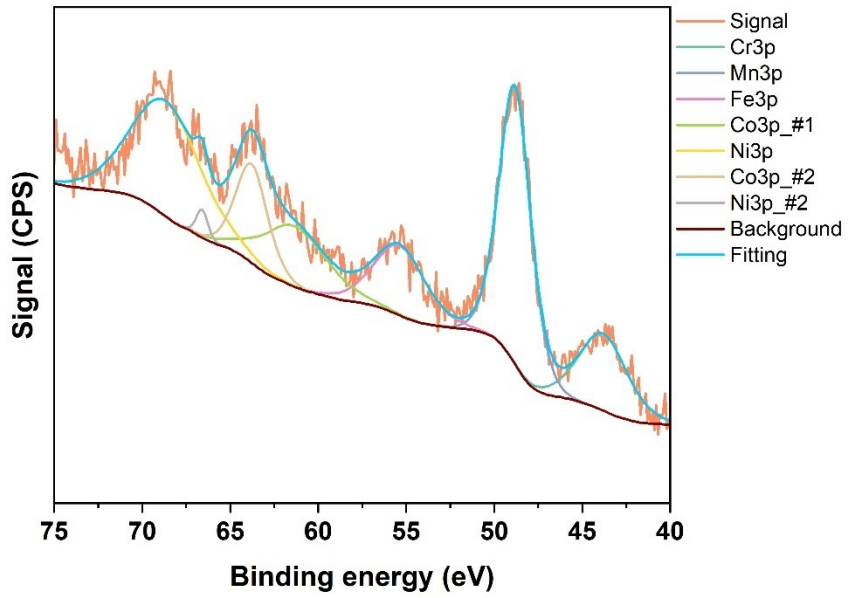

Figure S15 Deconvoluted 3p XPS spectra of as-synthesized HEA NPs in acetonitrile.

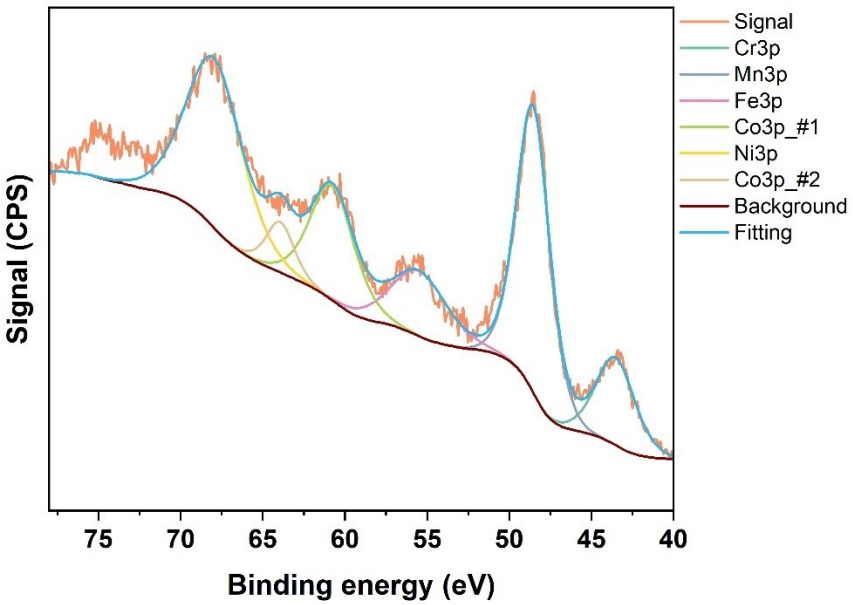

Figure S16 Deconvoluted 3p XPS spectra of as-synthesized HEA NPs in acetone.

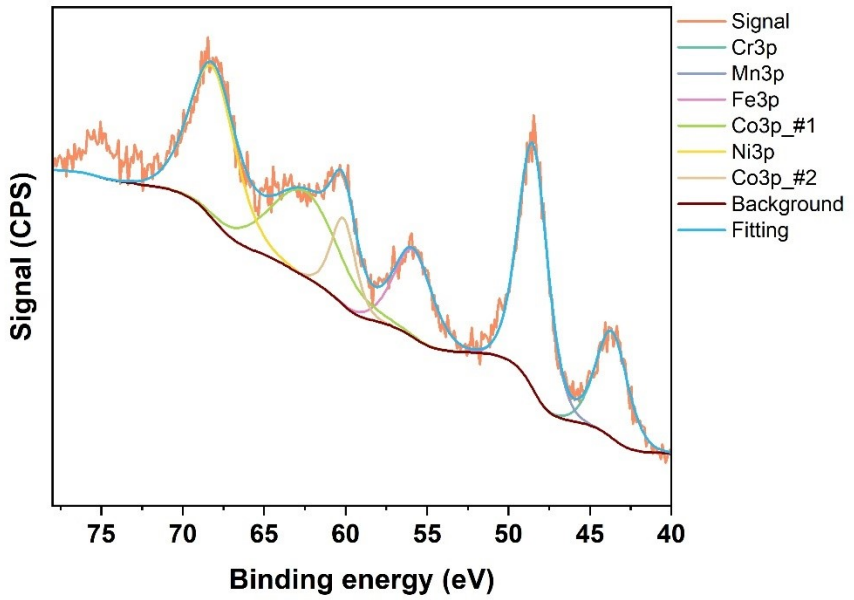

Figure S17 Deconvoluted 3p XPS spectra of as-synthesized HEA NPs in ethanol.

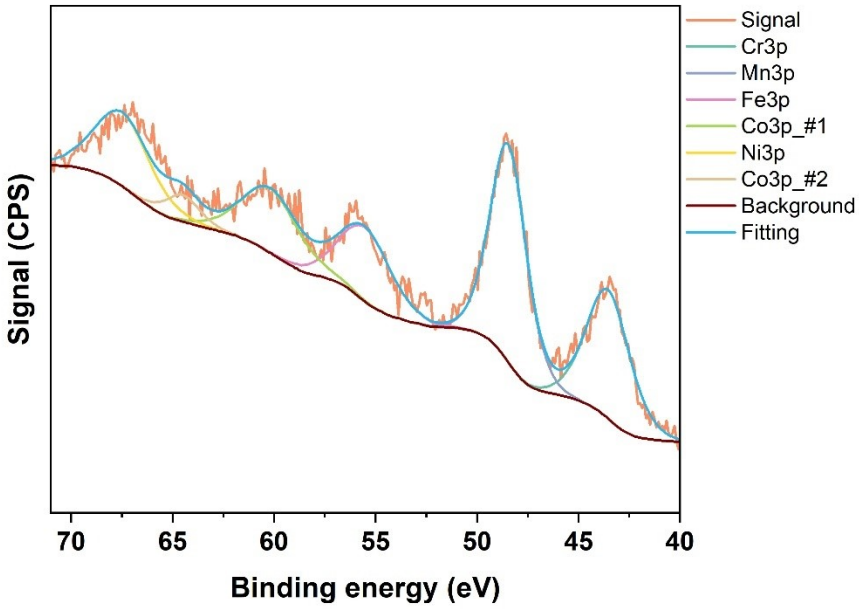

Figure S18 Deconvoluted 3p XPS spectra of annealed HEA NPs in acetonitrile.

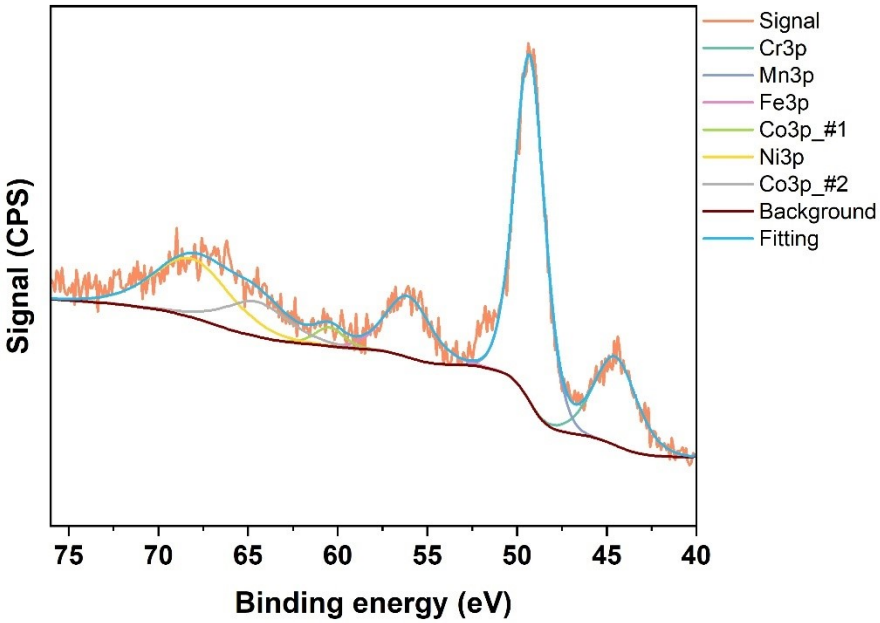

Figure S 19 Deconvoluted 3p XPS spectra of annealed HEA NPs in acetone.

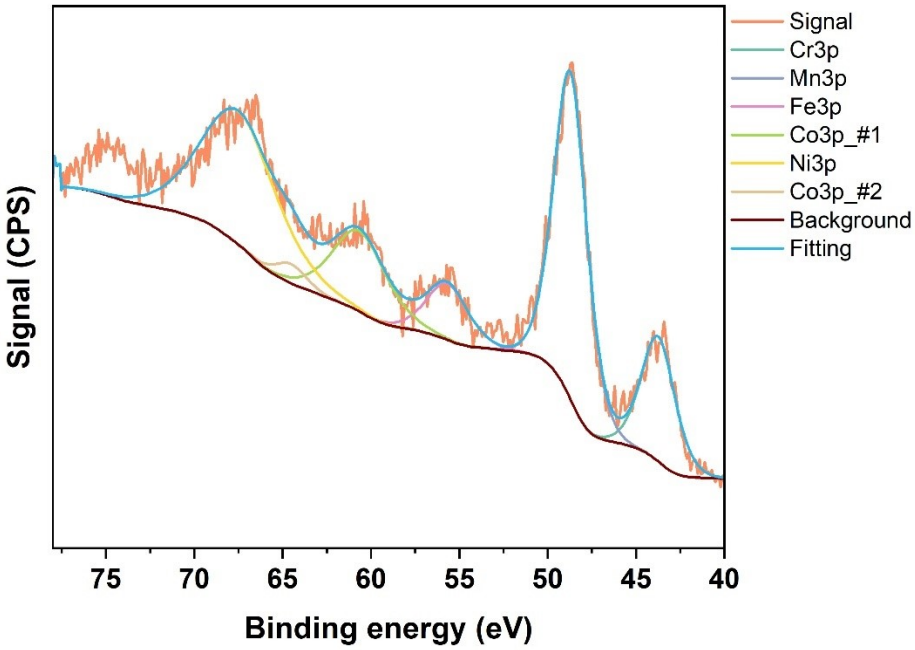

Figure S20 Deconvoluted 3p XPS spectra of annealed HEA NPs in ethanol.

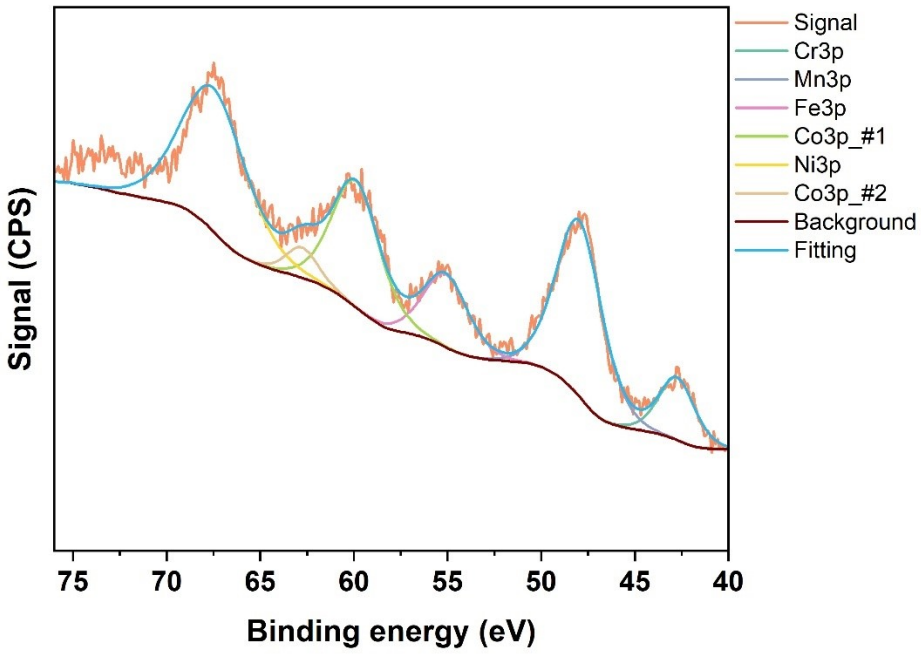

Figure S21 Deconvoluted 3p XPS spectra of annealed and electrochemically tested HEA NPs in acetonitrile.

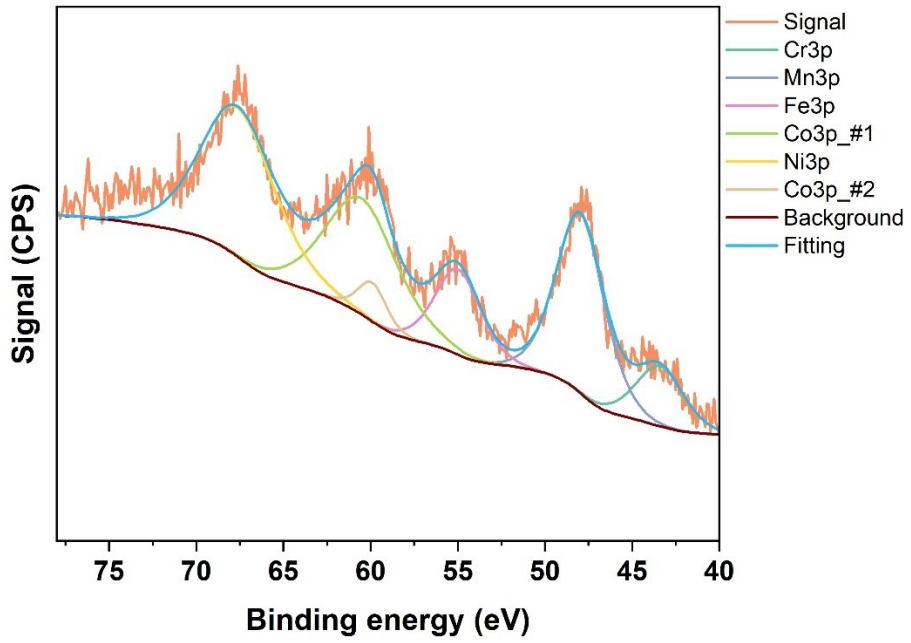

Figure S22 Deconvoluted 3p XPS spectra of annealed and electrochemically tested HEA NPs in acetone.

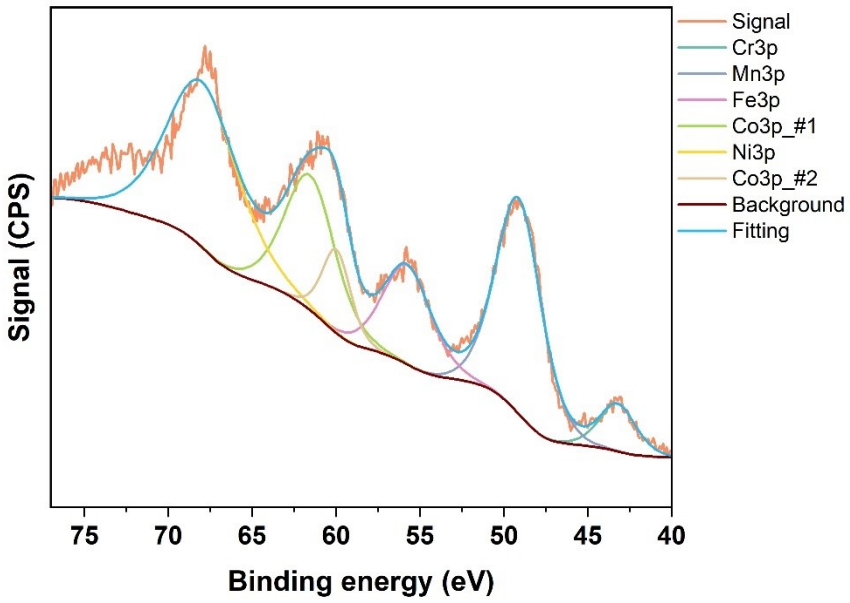

Figure S23 Deconvoluted 3p XPS spectra of annealed and electrochemically tested HEA NPs in ethanol.

References

[1] P. Chakthranont, J. Kibsgaard, A. Gallo, J. Park, M. Mitani, D. Sokaras, T. Kroll, R. Sinclair, M.B. Mogensen, T.F. Jaramillo, Effects of Gold Substrates on the Intrinsic and Extrinsic Activity of High-Loading Nickel-Based Oxyhydroxide Oxygen Evolution Catalysts, ACS Catal. 7 (2017) 5399–5409. https://doi.org/10.1021/acscatal.7b01070.

[2] A.R.C. Bredar, A.L. Chown, A.R. Burton, B.H. Farnum, Electrochemical Impedance Spectroscopy of Metal Oxide Electrodes for Energy Applications, ACS Appl. Energy Mater. 3 (2020) 66–98. https://doi.org/10.1021/acsaem.9b01965.